CrystEngComm

ROYAL SOCIETY
OF CHEMISTRY

PAPER
Suli Wu *et al.*
Photon upconversion of Nd³⁺–Yb³⁺–Tb³⁺ doped
core–shell–shell–shell nanoparticles

Photon upconversion of Nd³⁺–Yb³⁺–Tb³⁺ doped core–shell–shell–shell nanoparticles†

Wenfei Xun,[a] Zhipeng Meng,*[b] Chuwei Xie[c] and Suli Wu [iD] *[a]

808 nm excited Nd³⁺ doped upconversion nanoparticles (UCNPs) have become a new research hotspot due to their reduced thermal effect when applied in a water-rich system. Different from Tm³⁺-mediated energy migration upconversion of Tb³⁺, in this work, $NaYF_4$:Yb/Tb@$NaYF_4$:Yb@$NaNdF_4$:Yb@$NaYF_4$ core–shell–shell–shell nanoparticles were designed based on the Yb³⁺ sensitized cooperative energy-transfer process to realize photon upconversion. $NaYF_4$:Yb served as the migration layer, separating the activator Tb³⁺ from the sensitizer Nd³⁺ and minimizing the deleterious cross-relaxation between them. At 40% Yb³⁺ doping concentration in the $NaYF_4$:Yb layer, bright green luminescence was achieved under 808 nm excitation. Meanwhile, the presence of Yb³⁺ in the sensitization layer ($NaNdF_4$:Yb) reduced Nd³⁺ cross-relaxation, leading to improved energy migration efficiency of Nd³⁺ → Yb³⁺. Finally, the incorporation of an inert $NaYF_4$ shell resulted in a significant luminescence boost. These nanoparticles can be dispersed in water after surface modification and could be effectively excited after laser penetration of 3 cm of water, indicating the enormous potential of the designed UCNPs in the biological system.

Introduction

Lanthanide-doped UCNPs can absorb two or more photons and emit a single photon with a shorter wavelength.[1] Anti-Stokes-shifted luminescent materials have been widely applied in displays, anti-counterfeiting, biological labelling, and other fields due to their sharp emission bands, high light stability, and low biological toxicity.[2–7] Compared to typically 980 nm excited $NaYF_4$:Yb/Er or $NaYF_4$:Yb/Tm UCNPs, in which Er³⁺ or Tm³⁺ ions serve as activators and Yb³⁺ ions are used as sensitizers to absorb 980 nm NIR light,[6,8–14] Nd³⁺ doped UCNPs can be excited by an 808 nm laser and then transfer energy to the activator (for example, Er³⁺) through Yb³⁺ as an energy transfer bridge (Nd³⁺ → Yb³⁺ → Er³⁺),[15,16] greatly reducing the thermal effect caused by the strong absorption of water under 980 nm excitation. However, the inherently weak energy transfer efficiency limits their further applications. Researchers have tried to utilize different strategies such as changing the host lattice, energy transfer, surface passivation, surface plasmon coupling, and photonic crystals to modulate rare-earth luminescence.[17–27] For

example, Yan *et al.* built a $NaGdF_4$:Yb/Er@$NaGdF_4$:Nd/Yb core–shell structure, in which Er³⁺ and Nd³⁺ were doped separately in the core and shell, and the energy back transfer process can be inhibited through spatial separation.[28] Furthermore, Yao *et al.* synthesized sandwich-structured nanoparticles (NPs) including a $NaYF_4$:Yb quenching-shield layer between the activator core and Nd³⁺ doped shell.[29] The quenching-shield layer eliminated the energy transfer between Nd³⁺ and activators at the core–shell interface. On the other hand, Yb³⁺ doped in the quenching-shield layer transferred the excitation energy from the outside shell to the core, reducing deleterious energy back transfer. These methods allow for the doping of high concentrations of Nd³⁺ in the shell layer to achieve higher absorption efficiency.[29,30]

Although Tb³⁺ has typical green emission, compared to Yb–Er and Yb–Tm, Yb–Tb ion pairs are less used for achieving efficient upconversion luminescence (UCL) in rare earth fluorides due to the short lifetime of the intermediate level of Tb³⁺.[31] There are two main strategies to realize UCL of Tb³⁺. One is Tm/Gd energy migration-mediated upconversion (EMU). For example, Liu *et al.* reported $NaGdF_4$:Yb/Tm@$NaGdF_4$:Tb core–shell nanoparticles. Utilizing high-energy excited states of Tm, the excitation energy is transferred through Yb³⁺ → Tm³⁺ → Gd³⁺ and finally transferred to the Tb³⁺ in the shell layer through Gd sublattice-mediated energy migration.[32] A $NaGdF_4$:Tb@$NaGdF_4$:Yb/Tm@$NaGdF_4$:Yb/Nd core–shell–shell structure was also prepared to realize UCL under 808 nm *via* spatial separation of Nd³⁺, Tm³⁺, and Tb³⁺ to suppress

[a] State Key Laboratory of Fine Chemicals, Dalian University of Technology, 2# Linggong Road, Dalian 116024, P.R. China. E-mail: wusuli@dlut.edu.cn
[b] School of Chemistry and Chemical Engineering, Shandong University of Technology, Zibo 255049, P.R. China. E-mail: mengzhipeng@sdut.edu.cn
[c] School of Chemistry, Dalian University of Technology, 2# Linggong Road, Dalian 116024, P.R. China
† Electronic supplementary information (ESI) available. See DOI: https://doi.org/10.1039/d4ce00373j

nonradiative decays.[33] But the characteristic emission of Tm[3+] inevitably appeared in the UCL spectrum of Tb[3+]. The other strategy is the Yb[3+] sensitized cooperative energy-transfer (CET) process. Yan and Sun *et al.* prepared NaGdF$_4$:Yb/A@NaGdF$_4$:Nd/Yb (A = Tb, Eu), with Yb[3+] having a higher virtual excited state, which can match the energy diagram of Tb[3+] and Eu^{3+} to achieve green or red emission,[34] showing the unique advantages in realizing pure Tb[3+] luminescence.

In this work, a NaYF$_4$:Yb/Tb (20%/2%)@NaYF$_4$:Yb(40%)@NaNdF$_4$:Yb(10%)@NaYF$_4$ core–shell–shell–shell (CSSS) structure was designed to investigate the UCL of Tb[3+] under 808 nm NIR excitation. As illustrated in Scheme 1, Tb[3+] was doped in the inner core (Tb-core: NaYF$_4$:Yb/Tb), and sensitizer Nd[3+] was doped in the sensitization layer (Nd-layer: NaNdF$_4$:Yb). Sensitizer Nd[3+] and activator Tb[3+] were separated by an energy migration layer (Yb-layer: NaYF$_4$:Yb). On the one hand, the excited energy absorbed by Nd[3+] could sensitize the co-doped Yb[3+] in the Nd-layer by energy transfer (ET) and activated Tb[3+] through energy migration (EM) of the Yb-layer, thereby achieving UCL of Tb[3+]. On the other hand, the negative impact of Tb[3+] → Nd[3+] energy back transfer occurring at the core–shell interface can be ignored compared to the core–shell structure without a migration layer, improving the brightness of UCL. Meanwhile, the doping concentration of Yb[3+] ions in the Yb-layer was also investigated to optimize luminous intensity. Finally, an inert NaYF$_4$-shell (Y-layer) was encapsulated on the structure to further enhance the luminescence by reducing the surface quenching effect. These particles can be effectively excited by an 808 nm laser and display bright green luminescence ($^5D_4 \rightarrow {}^7F_5$), demonstrating great potential for applications in the fields of displays and life sciences.

Experimental

Materials

Yttrium(III) acetate hydrate (99.9%), ytterbium(III) acetate hydrate (99.9%), neodymium(III) acetate hydrate (99.9%), terbium(III) acetate hydrate (99.9%), oleic acid (AR) and 1-octadecene (90.0%) were purchased from Aladdin. Sodium hydroxide (NaOH; >96%) and polyethylene glycol ($n = 6000$) were purchased from TianDa Chemical Reagent Co., Ltd. and
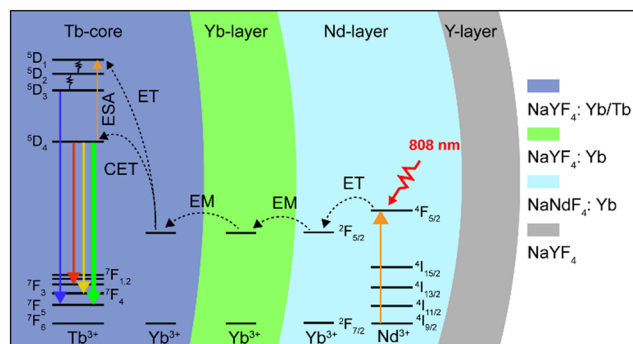

Scheme 1 Energy transfer mechanisms in the CSSS nanoparticle under 808 nm laser excitation.

ammonium fluoride (NH$_4$F; >96%) was purchased from Damao Chemical Reagent Factory. Cyclohexane was purchased from Tianjin Jindong Tianzheng Fine Chemical Reagent Factory. 2-Hydroxyethyl methacrylate (HEMA), acrylamide (AAm), ethylene glycol dimethacrylate (EGDMA), and 2′-hydroxy-1′-acetonaphthone (Darocur 1173) were purchased from Shanghai Macklin Biochemical Co., Ltd.

Synthesis procedures

Synthesis of the NaYF$_4$:20%Yb/2%Tb/x%Nd core NPs. The NaYF$_4$:20%Yb/2%Tb/x% Nd NPs were prepared *via* the coprecipitation method.[35] In a typical experiment for the synthesis of NaYF$_4$:20%Yb/2%Tb/1%Nd NPs, 0.616 mmol of Y(CH$_3$COOH)$_3$, 0.16 mmol of Yb(CH$_3$COOH)$_3$, 0.016 mmol of Tb(CH$_3$COOH)$_3$ and 0.008 mmol of Nd(CH$_3$COOH)$_3$ were added to a 100 mL three-necked flask containing 4 mL oleic acid and 16 mL 1-octadecene. The mixture was heated at 150 °C for 40 min. After cooling down to 50 °C, 4 mL NaOH methanol solution and 6.6 mL NH$_4$F methanol solution were added into the flask and stirred at 50 °C for 30 min. The solution was heated at 300 °C under a N$_2$ flow for 2 h and then was cooled down to room temperature. The NPs were separated by centrifugation, washed with ethanol three times, and finally dispersed in 5 mL cyclohexane. The synthetic sequence of the NaYF$_4$:20%Yb/2%Tb/x%Nd (x = 0, 0.5, 5) NPs was identical to the synthesis of the NaYF$_4$:20%Yb/2%Tb/1%Nd core NPs except for the ratio of the different rare earth acetates.

Synthesis of the NaYF$_4$:Yb/Tb@NaYF$_4$:y%Yb core–shell NPs. The NaYF$_4$:Yb/Tb@NaYF$_4$:y%Yb NPs were prepared *via* the coprecipitation method using the pre-synthesized core NPs as seeds. In a typical experiment for the synthesis of NaYF$_4$:Yb/Tb@NaYF$_4$:20%Yb NPs, 0.64 mmol of Y(CH$_3$COOH)$_3$ and 0.16 mmol of Yb(CH$_3$COOH)$_3$ were added to a 100 mL three-necked flask containing 4 mL oleic acid and 16 mL 1-octadecene. The mixture was heated at 150 °C for 40 min. The NaYF$_4$:20%Yb/2%Tb core NPs were added as seeds. After cooling down to 50 °C, 4 mL NaOH methanol solution and 6.6 mL NH$_4$F methanol solution were added into the flask and stirred at 50 °C for 30 min. The solution was heated at 300 °C under a N$_2$ flow for 2 h and then was cooled down to room temperature. The NPs were separated by centrifugation, washed with ethanol three times, and finally dispersed in 5 mL cyclohexane. The synthetic sequence of the NaYF$_4$:Yb/Tb@NaYF$_4$:y%Yb (y = 10, 40, 60, 80, 100) NPs was identical to the synthesis of the NaYF$_4$:Yb/Tb@NaYF$_4$:20%Yb NPs except for the different amounts of Yb(CH$_3$COOH)$_3$.

Synthesis of the NaYF$_4$:Yb/Tb@NaYF$_4$:y%Yb@NaNdF$_4$:Yb core–shell–shell NPs. The NaYF$_4$:Yb/Tb@NaYF$_4$:y%Yb@NaNdF$_4$:Yb NPs were prepared *via* the coprecipitation method using the pre-synthesized core–shell NPs as seeds. In a typical experiment for the synthesis of NaYF$_4$:Yb/Tb@NaYF$_4$:20%Yb@NaNdF$_4$:Yb NPs, 0.72 mmol of Nd(CH$_3$COOH)$_3$ and 0.08 mmol of Yb(CH$_3$COOH)$_3$ were added to a 100 mL three-necked flask containing 4 mL oleic acid and 16 mL 1-octadecene. The mixture was heated at 150 °C for 40 min. The

$NaYF_4$:Yb/Tb@$NaYF_4$:y%Yb core–shell NPs were added as seeds. After cooling down to 50 °C, 4 mL NaOH methanol solution and 6.6 mL NH_4F methanol solution were added into the flask and stirred at 50 °C for 30 min. The solution was heated at 300 °C under a N_2 flow for 2 h and then was cooled down to room temperature. The NPs were separated by centrifugation, washed with ethanol three times, and finally dispersed in 5 mL cyclohexane. The synthetic sequence of the $NaYF_4$:Yb/Tb@$NaYF_4$:y%Yb@$NaNdF_4$:Yb (y = 10, 40, 60, 80, 100) NPs was identical to the synthesis of the $NaYF_4$:Yb/Tb@$NaYF_4$:y%Yb core–shell NPs except for the different core–shell NPs used as seeds.

Synthesis of the $NaYF_4$:Yb/Tb@$NaYF_4$:y%Yb@$NaNdF_4$: Yb@$NaYF_4$ core–shell–shell–shell NPs. The $NaYF_4$:Yb/ Tb@$NaYF_4$:y%Yb@$NaNdF_4$:Yb@$NaYF_4$ NPs were prepared *via* the coprecipitation method using the pre-synthesized core–shell NPs as seeds. In a typical experiment for the synthesis of $NaYF_4$:Yb/Tb@$NaYF_4$:20%Yb@$NaNdF_4$:Yb@$NaYF_4$ NPs, 0.8 mmol of $Y(CH_3COOH)_3$ was added to a 100 mL three-necked flask containing 4 mL oleic acid and 16 mL 1-octadecene. The mixture was heated at 150 °C for 40 min. The $NaYF_4$:Yb/ Tb@$NaYF_4$:20%Yb@$NaNdF_4$:Yb core–shell–shell NPs were added as seeds. After cooling down to 50 °C, 4 mL NaOH methanol solution and 6.6 mL NH_4F methanol solution were added into the flask and stirred at 50 °C for 30 min. The solution was heated at 300 °C under a N_2 flow for 2 h and then was cooled down to room temperature. The NPs were separated by centrifugation, washed with ethanol three times, and finally dispersed in 5 mL cyclohexane. The synthetic sequence of the $NaYF_4$:Yb/Tb@$NaYF_4$:y%Yb@$NaNdF_4$:Yb@$NaYF_4$ (y = 10, 40, 60, 80, 100) NPs was identical to the synthesis of the $NaYF_4$:Yb/ Tb@$NaYF_4$:20%Yb@$NaNdF_4$:Yb@$NaYF_4$ NPs except for the different core–shell–shell NPs used as seeds.

Surface modification of the core–shell–shell–shell NPs. Firstly, UCNPs were centrifuged to obtain the solid, 0.1 g of polyethylene glycol (n = 6000) was dissolved in 10 ml of deionized water, and the solid was added to the polyethylene glycol solution and placed in an ultrasonicator until the NPs were evenly dispersed in the solution.

Fabrication of hydrogel. First, 4.68 M AAm and 4.65 M HEMA were mixed in DI solvent and then EGDMA and Darocur 1173 were added with a weight ratio of 0.57 and 0.17 wt% relative to AAm, respectively. The above precursor solution was infiltrated into the 700 μm-thick gap by capillary force and was illuminated by a UV lamp for 30 min.

Characterization

High-resolution transmission electron microscopy and element mapping observations were performed on a JEM-F200 (200 kV). The upconversion luminescence spectra were recorded on an FLS-920 fluorescence spectrum instrument with an external 808 nm or 980 nm semiconductor laser (MDL-III-808 nm, MDL-III-980 nm, Changchun New Industries Optoelectronics Technology Co., Ltd., China). X-ray diffraction (XRD) spectra were recorded on a SmartLab 9 kW solid powder diffractometer.

Results and discussion

To prepare the designed UCNPs, a layer-by-layer synthesis process was performed. $NaYF_4$:Yb/Tb core NPs were first synthesized *via* the reported coprecipitation method.[35] The TEM images in Fig. 1a and S1a† show that monodisperse core NPs with ~20 nm size were obtained. Then, the Yb-layer ($NaYF_4$:Yb) with about 5 nm thickness was coated on the core to form core–shell (CS) NPs (Fig. 1b and S1b†). Both the core and the CS NPs exhibit a uniform hexagonal prism morphology. Then the Nd-layer was grown, which only can selectively grow along the long axis of $NaYF_4$ crystals due to the lattice mismatch between the $NaYF_4$ and $NaNdF_4$, leading to oblong core–shell–shell (CSS) nanostructures (Fig. 1c).[36,37] Subsequently, the CSS NPs were coated with an inert $NaYF_4$ layer to form the designed core–shell–shell–shell (CSSS) NPs (Fig. 1d) with a diameter of 70 nm (Fig. S1d†). The high-resolution TEM (HRTEM) image with a typical *d* spacing of about 0.52 nm (Fig. 1e) was consistent with the $\{10\bar{1}0\}$ crystal plane spacing of the hexagonal phase reported.[38] Meanwhile, the fast Fourier transform (FFT) of the lattice (Fig. 1f) and the XRD pattern in Fig. S2† further revealed its hexagonal phase characteristics. The corresponding element mapping in Fig. 1g illustrates the distributions of different doped ions, where the higher Nd in the middle region is consistent with the design compositions for the CSSS particles.

To verify the rationality of the structural design, we first investigated the importance of the spatial separation of the dopant ions Nd^{3+} and Tb^{3+}. As shown in Fig. 2a, compared to $NaYF_4$:Tb/Nd/Yb, the $NaYF_4$:Yb/Tb@$NaNdF_4$:Yb CS structure
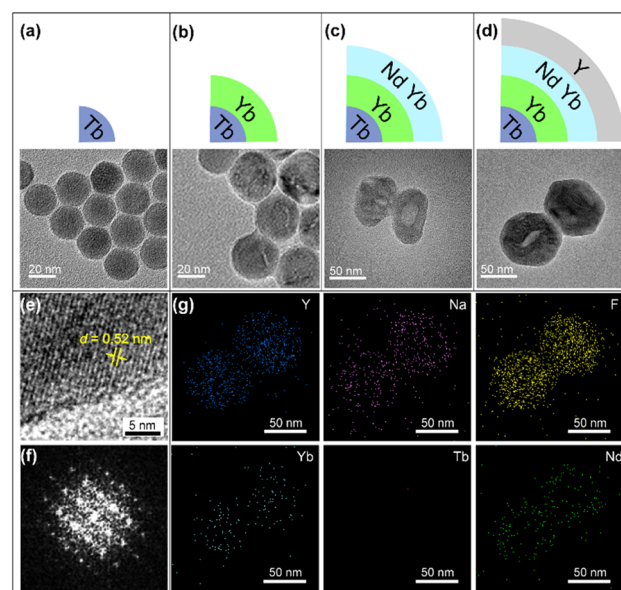
Fig. 1 Scheme and TEM images of the as-prepared nanoparticles: (a) core $NaYF_4$:Yb/Tb NPs, (b) $NaYF_4$:Yb/Tb@$NaYF_4$:Yb NPs, (c) $NaYF_4$:Yb/ Tb@$NaYF_4$:Yb@$NaNdF_4$:Yb NPs and (d) $NaYF_4$:Yb/Tb@$NaYF_4$: Yb@$NaNdF_4$:Yb@$NaYF_4$ NPs. (e and f) HRTEM images of CSSS NPs and their fast Fourier transform (FFT) pattern. (g) Element mappings of Y, Na, F, Yb, Tb, and Nd for CSSS NPs shown in (d).

(Yb/Tb@Nd/Yb) produced visible green luminescence after excitation, demonstrating that the cross-relaxation process greatly quenched the luminescence when Nd^{3+} and Tb^{3+} were co-doped in the same layers. Furthermore, the CSS NPs (Yb/Tb@Yb@Nd/Yb) obtained an improved luminescence intensity by introducing an energy migration layer to prevent the deleterious cross-relaxation and energy back transfer of $Tb^{3+} \rightarrow Nd^{3+}$, allowing the energy of the excited Nd^{3+} ions to be transferred to the core layer to excite Tb^{3+} ions. Finally, an inert $NaYF_4$ shell was coated on the CSS NPs, referred to as Yb/Tb@Yb@Nd/Yb@Y, to eliminate the surface quenching and greatly improve the brightness of the luminescence. The finally obtained UCNPs displayed typical 415 ($^5D_3 \rightarrow {}^7F_5$), 543 ($^5D_4 \rightarrow {}^7F_5$) and 584 ($^5D_4 \rightarrow {}^7F_4$) nm emission bands of Tb^{3+} under 808 nm excitation. The emissions at 525 and 658 nm should be assigned to impurity Er^{3+} ions mixed in the ytterbium acetate reagent. The emission at 477 nm was consistent with the previously reported cooperative luminescence from a pair of Yb^{3+} ions in the excited state.[39] Meanwhile, the UCNPs can also be excited by a 980 nm laser. The photograph and luminescence spectrum in Fig. S3† show that similar luminescence was achieved under 808 and 980 nm laser excitation, respectively, illustrating the excellent energy transfer efficiency of the structure.

To investigate the upconversion mechanism, the number of photons involved in the transition process was obtained using the logarithmic fit of luminescence intensity–power (I–P). As shown in Fig. 2b, the $^5D_4 \rightarrow {}^7F_5$ and $^5D_4 \rightarrow {}^7F_4$ transitions of Tb^{3+} followed two-photon processes, while the $^5D_3 \rightarrow {}^7F_5$ transition followed three-photon processes, which is well correlated to the proposed energy transfer (Scheme 1) *via* the Yb^{3+}-based CET process.[40–42]

According to the luminescence mechanism, a series of NPs doped with different concentrations of Yb^{3+} in the Yb-layer (from 10 to 100 mol%) were synthesized and their UCL spectra were recorded as shown in Fig. 3a. With the increase of doping concentration, the intensity of UCL was greatly enhanced first, and the strongest green luminescence was generated at the 40% Yb^{3+}-doped structure. The result reveals

that a high concentration of Yb^{3+} ions is required to activate the energy migration process.[43] However, when the Yb^{3+} doping concentration was further increased, the UCL intensity decreased (Fig. 3a). The corresponding digital photos in Fig. 3b also demonstrated that the optimal luminous brightness occurs at 40% Yb^{3+} doping concentration in the Yb-layer. To detect the relaxation process during energy transfer, we synthesized $NaYF_4$:m%Yb@$NaNdF_4$:Yb@$NaYF_4$ NPs and detected the emission lifetime at 980 nm (Yb^{3+} $^2F_{5/2}$ level) under 808 nm excitation. When 40% Yb^{3+} was doped in the $NaYF_4$:m%Yb core, the lifetime of Yb^{3+} was longer than that when 100% Yb^{3+} was doped (Fig. S5†), indicating the energy back transfer from Yb^{3+} to Nd^{3+} when 100% Yb^{3+} was doped. In addition, in CSSS UCNPs, the lifetime at 543 nm (Tb^{3+} $^5D_4$ level) increased with increasing Yb^{3+} doping concentration in the Yb-layer (Fig. S6†), which was consistent with the energy cycle (EC) process between Yb^{3+} ions,[44] indicating that the EC process was a pathway leading to energy loss.

To further understand the role of Yb sublattice energy migration, $NaYF_4$:Yb/Tb@$NaYF_4$:Yb@$NaNdF_4$ (Yb/Tb@Yb@Nd) without Yb^{3+} in the Nd-layer was synthesized. The luminescence of Yb/Tb@Yb@Nd cannot be detected under 808 nm (Fig. 4a). In this case, direct $Nd^{3+} \rightarrow Yb^{3+}$ energy transfer only occurred at the core–shell interface (interfacial energy transfer, IET).[45] Meanwhile, the multiple $Nd^{3+} \rightarrow Nd^{3+}$ EM processes with cross-relaxation in the sensitization layer caused non-radiative energy loss,[46] thereby reducing the luminescence intensity greatly (Fig. 4a). For the Yb/Tb@Yb@Nd/Yb NPs, the Yb^{3+} ions doped in the sensitization shell can effectively collect the excitation energy of the nearby Nd^{3+} ions through the ET process of $Nd^{3+} \rightarrow Yb^{3+}$ and transfer to the Tb-core through the Yb sublattice EM procedure (Fig. 4b),[47] and the energy loss was greatly reduced due to the simple excited state ($^2F_{5/2}$) of Yb^{3+} ions in this process.[48] Hence, co-doped Yb^{3+} in the energy migration layer is essential to improve UCL.

We investigate the possibility of CSSS UCNPs for use in water-rich environments by inserting a cuvette containing deionized water between the UCNPs and the laser (Fig. 5a). UCNPs can still be activated when an 808 nm laser passed through 4 cm of water (Fig. 5b). Furthermore, surface
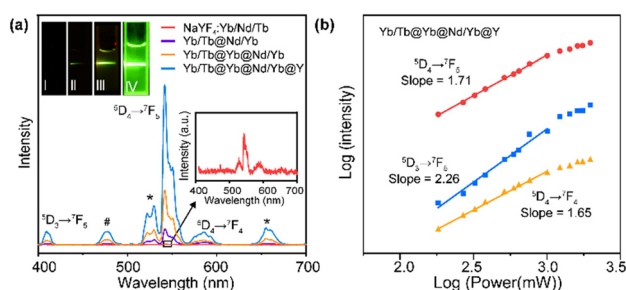

Fig. 2 (a) UCL spectra of $NaYF_4$:Yb/Nd/Tb, Yb/Tb@Nd/Yb, Yb/Tb@Yb@Nd/Yb and Yb/Tb@Yb@Nd/Yb@Y NPs. Symbol "*" represents the emission peaks assigned to Er^{3+} and symbol "#" represents the emission peak assigned to Yb^{3+}. Insert: Digital photographs of $NaYF_4$:Yb/Nd/Tb, Yb/Tb@Nd/Yb, Yb/Tb@Yb@Nd/Yb and Yb/Tb@Yb@Nd/Yb@Y NPs under 808 nm excitation. (b) Logarithmic fit of luminescence intensity–power of CSSS NPs excited by 808 nm NIR.
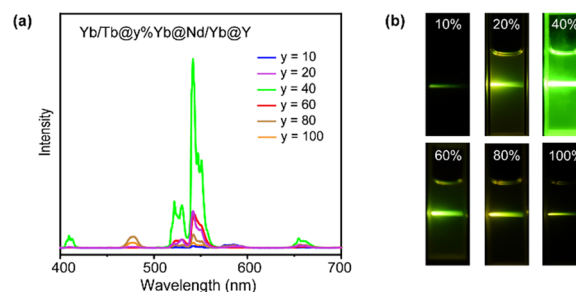

Fig. 3 (a) Upconversion luminescence spectra of Tb/Yb@y%@Nd/Yb@Y (y = 10–100) CSSS NPs. (b) Digital photos of Tb/Yb@y%Yb@Nd/Yb@Y (y = 10–100) CSSS NPs.
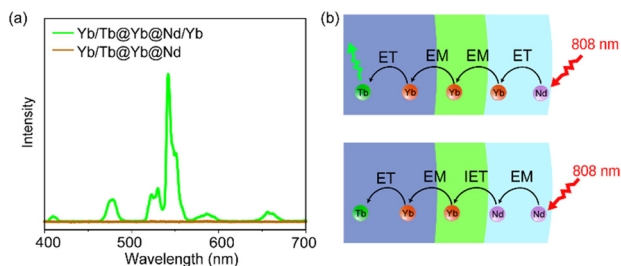
Fig. 4 (a) Upconversion luminescence spectra of Tb/Yb@Yb@Nd/Yb and Tb/Yb@Yb@Nd CSS NPs. (b) Scheme of the CSS structure and energy transfer processes.
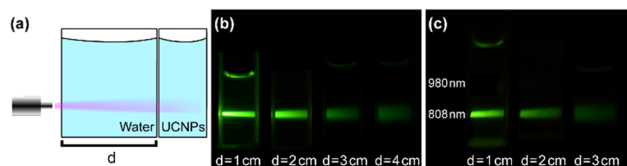

Fig. 5 (a) Schematic diagram of excitation of surface modified UCNPs by an 808 nm laser penetrating water. (b) The digital photos of UCL of CSSS NPs excited by the 808 nm laser after passing through 1–4 cm water. (c) The digital photos of UCL of surface modified CSSS NPs dispersed in deionized water excited by 980 nm and 808 nm lasers after passing through 1–3 cm water.

modification of CSSS UCNPs was carried out using polyethylene glycol, and the surface modified UCNPs could be dispersed in deionized water. The digital photos in Fig. 5c showed UCL of surface modified UCNPs dispersed in deionized water after 980 nm and 808 nm laser penetration of 1–3 cm water. The surface modified UCNPs could still be excited after the 808 nm laser passed through 3 cm water and could not be excited after the 980 nm laser penetrated 1 cm of water. This finding highlights the enormous potential of Nd^{3+}-doped materials in the application field of biology. The thermal effect of the laser in the water-rich environment was measured using P(AAm-HEMA) hydrogel as a biological model. The temperature of the hydrogel heated by the 808 nm laser was raised from 14.9 °C to 15.6 °C, while the hydrogel under the 980 nm laser was heated to 38.6 °C after 360 s exposure (Fig. S6a and b†).

Conclusions

Based on the Yb^{3+} sensitized cooperative energy-transfer upconversion mechanism, we designed and synthesized $NaYF_4:Yb/Tb@NaYF_4:Yb@NaNdF_4:Yb@NaYF_4$ CSSS NPs that exhibit distinctive upconversion luminescence of Tb^{3+} when excited by an 808 nm laser. After comparing various Nd^{3+} and Yb^{3+} doped structures, we confirmed that effective UCL was achieved by introducing a migration layer between the Tb-core and the sensitizer Nd-layer. The migration layer can prevent deleterious cross-relaxation between Nd^{3+} and Tb^{3+}, allowing the excited Nd^{3+} energy to be transferred to excite

Tb^{3+} ions ($Nd^{3+} \rightarrow Yb^{3+} \rightarrow Tb^{3+}$). Additionally, the ideal Yb^{3+} doping concentration in the Yb-layer was studied and the results indicated that the sample with 40% Yb^{3+} doping showed bright green fluorescence. Meanwhile, we found that co-doping the sensitization layer with Nd^{3+} and Yb^{3+} reduces cross-relaxation between Nd^{3+} ions and improves the energy transfer efficiency of $Nd^{3+} \rightarrow Yb^{3+}$. After surface modification, CSSS NPs could be dispersed in water and could be effectively excited after 808 nm laser penetration of 3 cm of water, demonstrating a promising future for 808 nm-stimulated UCNPs in water-rich settings, particularly in living tissues and cells.

Author contributions

Wenfei Xun: conceptualization, investigation, methodology, writing – original draft. Zhipeng Meng: writing – original draft, validation. Chuwei Xie: characterization. Suli Wu: conceptualization, investigation, methodology.

Conflicts of interest

There are no conflicts to declare.

Acknowledgements

References

1 O. Dukhno, S. Ghosh, V. Greiner, S. Bou, J. Godet, V. Muhr, M. Buchner, T. Hirsch, Y. Mély and F. Przybilla, *ACS Appl. Mater. Interfaces*, 2024, **16**, 11217–11227.

2 J. Xu, P. Yang, M. Sun, H. Bi, B. Liu, D. Yang, S. Gai, F. He and J. Lin, *ACS Nano*, 2017, **11**, 4133–4144.

3 Y. Li, S. Zeng and J. Hao, *ACS Nano*, 2019, **13**, 248–259.

4 M. Wang, J. Song, F. Zhou, A. R. Hoover, C. Murray, B. Zhou, L. Wang, J. Qu and W. R. Chen, *Adv. Sci.*, 2019, **6**, 1802157.

5 S. Hao, Y. Shang, Y. Hou, T. Chen, W. Lv, P. Hu and C. Yang, *Sol. Energy*, 2021, **224**, 563–568.

6 Y. L. Xiong, J. N. Guo, L. Yang, S. R. Yao, P. Xiao and Y. H. Zhang, *ACS Sustainable Chem. Eng.*, 2021, **9**, 11171–11178.

7 S. Natalia, R. Marcin, W. Przemysław, L. Stefan and P. Du, *NANO*, 2022, **12**, 799.

8 M. Gunaseelan, S. Yamini, G. A. Kumar and J. Senthilselvan, *Opt. Mater.*, 2018, **75**, 174–186.

9 F. Chen, Q. J. Lu, Y. Y. Zhang and S. Z. Yao, *Sens. Actuators, B*, 2019, **297**, 126751.

10 J. J. Zhang, S. L. Zhao, Z. Xu, L. G. Zhang, P. F. Zuo and Q. X. Wu, *RSC Adv.*, 2019, **9**, 3688–3692.

11 S. Z. Lv, K. Y. Zhang, L. Zhu and D. P. Tang, *Anal. Chem.*, 2020, **92**, 1470–1476.

12 G. Murali, S. Vattikuti, Y. K. Kshetri, H. Lee, J. Modigunta, C. S. Reddy, S. Park, S. Lee, B. Poornaprakash, H. Lee, Y. H. Park, J. Lee, S. Y. Park and I. In, *Chem. Eng. J.*, 2021, **421**, 129687.

13 E. M. Trifanova, M. E. Nikolaeva and V. K. Popov, *Inorg. Mater. Appl. Res.*, 2022, **13**, 426–433.

14 M. Vukovic, I. Dinic, P. Jardim, S. Markovic, L. Veselinovic, M. Nikolic and L. Mancic, *Adv. Powder Technol.*, 2022, **33**, 103403.

15 D. Wang, B. Xue, X. G. Kong, L. P. Tu, X. M. Liu, Y. L. Zhang, Y. L. Chang, Y. S. Luo, H. Y. Zhao and H. Zhang, *Nanoscale*, 2015, **7**, 190–197.

16 D. Q. Chen, M. Xu, P. Huang, M. F. Ma, M. Y. Ding and L. Lei, *J. Mater. Chem. C*, 2017, **5**, 5434–5443.

17 B. Liu, Z. Meng, S. Wu, Y. Wu and S. Zhang, *Nanoscale Horiz.*, 2018, **3**, 616–623.

18 Z. P. Meng, S. L. Wu and S. F. Zhang, *J. Mater. Chem. C*, 2018, **6**, 13101–13107.

19 X. S. Cui, Y. Cheng, H. Lin, Q. P. Wu, J. Xu and Y. S. Wang, *J. Rare Earths*, 2019, **37**, 573–579.

20 S. Tek, B. A. Vincent, L. C. Mimun, A. Ponce and K. L. Nash, *Cryst. Growth Des.*, 2020, **20**, 2153–2163.

21 J. M. Bi, H. Y. Sun, X. X. Ke, L. Xu, R. D. Liu, L. L. Zhu and R. Qiao, *J. Ind. Eng. Chem.*, 2023, **121**, 452–461.

22 F. Liu, Y. Q. Wang, S. C. Zhang, F. Sun, D. Xu, W. L. Wang, X. Y. Li, W. S. Yu, H. Yu and X. T. Dong, *Ceram. Int.*, 2023, **49**, 26589–26603.

23 Y. Ma, T. Wen, K. Liu, D. Jiang, M. Zhao, C. Lin and Y. Wang, *J. Mater. Chem. C*, 2023, **11**, 6588–6596.

24 Z. Meng, W. Xun, S. Zhang and S. Wu, *ACS Appl. Opt. Mater.*, 2023, **1**, 421–429.

25 A. Skripka, M. Lee, X. Qi, J. A. Pan, H. R. Yang, C. Lee, P. J. Schuck, B. E. Cohen, D. Jaque and E. M. Chan, *Nano Lett.*, 2023, **23**, 7100–7106.

26 H. Wang, Z. He, K. Cai, L. M. Wei, Y. Xu, Y. Fu, M. M. Xing and Y. Tian, *Chem. Eng. J.*, 2023, **468**, 143558.

27 X. M. Yin, Q. Xiao, L. Lv, X. Y. Wu, X. Y. Dong, Y. Fan, N. Zhou and X. X. Luo, *Spectrochim. Acta, Part A*, 2023, **291**, 122324.

28 Y. Wang, G. Liu, L. Sun, J. Xiao, J. Zhou and C. Yan, *ACS Nano*, 2013, **7**, 7200–7206.

29 Y. Zhong, G. Tian, Z. Gu, Y. Yang, L. Gu, Y. Zhao, Y. Ma and J. Yao, *Adv. Mater.*, 2014, **26**, 2831–2837.

30 B. Liu, Y. Chen, C. Li, F. He, Z. Hou, S. Huang, H. Zhu, X. Chen and J. Lin, *Adv. Funct. Mater.*, 2015, **25**, 4717–4729.

31 B. Zhou, J. Huang, L. Yan, X. Liu, N. Song, L. Tao and Q. Zhang, *Adv. Mater.*, 2019, **31**, 1806308.

32 F. Wang, R. Deng, J. Wang, Q. Wang, Y. Han, H. Zhu, X. Chen and X. Liu, *Nat. Mater.*, 2011, **10**, 968–973.

33 T. Wang, H. F. Zhou, Z. C. Yu, G. J. Zhou, J. Zhou, D. P. Huang, L. L. Sun, P. Gao, Y. Z. Sun and J. F. Hu, *J. Phys. Chem. C*, 2018, **122**, 10113–10124.

34 H. Dong, L. Sun, Y. Wang, J. Xiao, D. Tu, X. Chen and C. Yan, *J. Mater. Chem. C*, 2016, **4**, 4186–4192.

35 F. Wang, R. Deng and X. Liu, *Nat. Protoc.*, 2014, **9**, 1634–1644.

36 H. Peng, B. Ding, Y. Ma, S. Sun, W. Tao, Y. Guo, H. Guo, X. Yang and H. Qian, *Appl. Surf. Sci.*, 2015, **357**, 2408–2414.

37 Z. Lei, X. Ling, Q. Mei, S. Fu, J. Zhang and Y. Zhang, *Adv. Mater.*, 2020, **32**, 1906225.

38 H. Mai, Y. Zhang, L. Sun and C. Yan, *J. Phys. Chem. C*, 2007, **111**, 13730–13739.

39 B. Lai, J. Wang and Q. Su, *Appl. Phys. B: Lasers Opt.*, 2010, **98**, 41–47.

40 J. Qiu, M. Shojiya, R. Kanno and Y. Kawamoto, *Opt. Mater.*, 1999, **13**, 319–325.

41 J. L. Adam, N. Duhamel-Henry and J. Y. Allain, *J. Non-Cryst. Solids*, 1997, **213–214**, 245–250.

42 R. C. Knighton, L. K. Soro, L. Francés-Soriano, A. Rodríguez-Rodríguez, G. Pilet, M. Lenertz, C. Platas-Iglesias, N. Hildebrandt and L. J. Charbonnière, *Angew. Chem., Int. Ed.*, 2022, **61**, e202113114.

43 F. Wang, R. Deng, J. Wang, Q. Wang, Y. Han, H. Zhu, X. Chen and X. Liu, *Nat. Mater.*, 2011, **10**, 968–973.

44 R. Sun, J. Li, J. Chen, Y. Xie and L. Sun, *Adv. Opt. Mater.*, 2024, 2302880.

45 B. Zhou, Q. Li, L. Yan and Q. Zhang, *J. Rare Earths*, 2020, **38**, 474–482.

46 J. Fan, L. Liang, Y. Gu and X. Liu, *Opt. Mater.: X*, 2021, **12**, 100104.

47 Y. Zhong, I. Rostami, Z. Wang, H. Dai and Z. Hu, *Adv. Mater.*, 2015, **27**, 6418.

48 X. Huang, *Opt. Lett.*, 2015, **40**, 3599–3602.